

**25<sup>th</sup> International Technical Conference on the Enhanced Safety of Vehicles**  
**June 5-8, 2017, Detroit, Michigan**  
**Paper ID# 17-0436**

**VALIDATION OF MATERIAL MODELS: DESIGN AND ANALYSIS OF COMPOSITE FRONT BUMPER CRUSH-CAN SYSTEM**

**Praveen Reddy Pasupuleti**  
**Mark Doroudian**  
**Ramesh Dwarampudi**  
ESI North America  
USA

**Alain Trameçon, Sebastian Müller**  
ESI Group  
France, Germany

**Anthony M. Coppola, Libby Berger**  
General Motors

**Derek Board, Omar Faruque**  
Ford Motor Company

**James Truskin**  
FCA USA LLC

**Manish Mehta**  
M-Tech International LLC

**ABSTRACT**

Composite materials provide an avenue to achieve weight savings in structural automotive components due to their low density, high structural performance, and excellent energy absorption during impact. However, many challenges exist in implementing composites in automotive applications, including manufacturing throughput, part quality, part cost and the relative immaturity of prediction capabilities during the design phase. The latter, in particular, can limit weight savings and increase cost by requiring oversized components and a reliance on extensive physical validation testing.

The Validation of Material Models for Crash of Carbon Fiber Composites project is a four-year Cooperative Agreement project between the U.S. Automotive Materials Partnership (USAMP) and the US Department of Energy (DOE). The primary objective is to validate and assess the ability of physics-based material models to predict crash performance of automotive primary load-carrying carbon fiber composite structures. Models evaluated include Automotive Composites Consortium/USAMP-developed models from the University of Michigan (UM) and Northwestern University (NWU), as well as four major commercial crash codes: LS-DYNA, RADIOSS, VPS (PAM-CRASH), and Abaqus. Predictions are compared with experimental results from quasi-static testing and dynamic crash testing of a lightweight

carbon fiber composite front-bumper and crush-can (FBCC) system which was selected for demonstration via design, analysis, fabrication, and crash testing. Performance targets and the physical design space for the composite FBCC system were derived from physical testing and virtual simulation of a surrogate steel FBCC. This paper will discuss the results from experimental testing and CAE predictions as well as the sources of gaps between them. Special focus will be placed on how these results can be used for design considerations of carbon fiber composite energy absorption systems.

## 1. **Background**

The objective of this four-year, \$7 million U.S. DOE and USAMP Cooperative Agreement project is to validate and assess the ability of physics-based material models to predict crash performance of automotive primary load-carrying carbon fiber composite structures.<sup>[1]</sup>

The usage of composites in the automotive industry is widely known, but to realize the effective performance of these composite structures under various load conditions potentially requires many crash tests. To avoid expensive trials, computer-aided engineering (CAE) simulations are used to reduce the number of trial and error procedures in developing a product.

Models evaluated include Automotive Composites Consortium / USAMP-developed models from the University of Michigan (UM) and Northwestern University (NWU), as well as more standard models from four major commercial crash simulation codes: LS-DYNA, RADIOSS, VPS (formerly called PAM-CRASH), and Abaqus. In this paper, will be compared results obtained with the state-of-the-art model used in VPS and the first implementation in VPS of the USAMP developed models.

Predictions are presently being compared to experimental results from quasi-static testing and dynamic crash testing of a lightweight carbon fiber composite Front-Bumper and Crush-Can (FBCC) system which was selected for demonstration via design, analysis, fabrication, and crash testing.

In the past, many researchers have worked on developing numerical models that predicts progressive damage and failure in fiber reinforced laminates [Ref 2, 7-8]. In this paper, such commercially available models were used with an attempt to design a composite FBCC within the steel packaging space that is mass producible, production feasible, predictable as steel with equivalent energy absorption to a steel FBCC.

The first step in developing the composite FBCC was to establish design targets based on a steel FBCC system. The existing steel FBCC was initially simulated under various crash loads to generate target energy absorption requirements. The steel FBCC simulations from CAE codes correlated reasonably well with experiments. Once the design targets were set for an equivalent composite FBCC, an iterative process via simulations was executed to optimize the composite design to fit within the set design space. Multiple iterations were conducted to optimize the shape of the components, evaluate competing manufacturing processes, type of material, layup sequence, attachment methods, etc. Firstly commercially available material models selected for crash analysis were validated against simple tension, compression and shear properties. Then additional tests were required to address the unique characterization requirements of Waas Pineda material model introduced in the project by University of Michigan and Northwestern University, and now available in VPS.

While two different materials (unidirectional (UD) and woven) laminates were tested and simulated, only woven composites were selected by the USAMP team for the design of the composite FBCC. Following coupon and

component level validations using hat section geometries, a full FBCC crash analysis under 6 different load conditions was executed. Key metrics being used to compare CAE to tests include: force versus deflection response, average crush force, crush distance, acceleration versus time response, and displacement versus time response and composite failure mechanisms.

The design also had a weight save target of >30 percent less than the steel FBCC. Unlike a steel assembly, the attachment of composite crush-cans to composite bumper cannot be performed via traditional welding or riveting techniques, and required a unique joining strategy to implement localized bonding on critical interfaces. A novel, patent-pending strategy was adopted to mold SMC backing plate material onto the rear end of crush-cans in order to effectively attach the full FBCC to the crash sled utilizing bolts. This paper describes the process for establishing design targets for the composite FBCC, achieving a manufacturable design of composite FBCC and developing predictions using VPS code.

## 2. Design Targets

The selected baseline steel FBCC design donated by Ford shown in Figure 1 was simulated under various load conditions (4 high speed and 2 low speed) using four different commercial codes i.e., (VPS, LS-DYNA, RADIOSS and Abaqus). The material data for different steel sub-components was supplied by Ford and is highlighted in Table 1. VPS MAT 103 Elastic-Plastic Iterative Hill was used for all deformable steel components. The provided plastic behavior for bumper and crush-can is shown in Figure 2 and 3. Strain rate dependency was only modeled for crush-cans, Figure 3. Material and spot weld failure were not considered in the

models. A series of high speed and low speed impact simulations were carried out in VPS as shown in Table 2.

Table 3 illustrates the key design targets for composite FBCC as derived from Steel FBCC predictions, which were collaboratively established by the VMM Project Design/CAE Team, comprised of a multi-disciplinary technical staff, in order to leverage critical mechanics, materials, processing, joining and NDE expertise amongst OEMs, suppliers and academics.

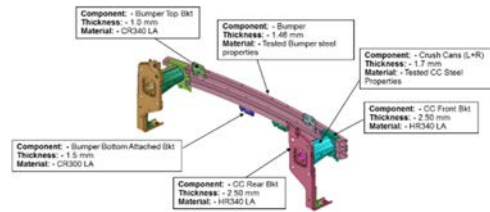


Figure 1. Steel FBCC Components

Table 1. Material Properties of Steel FBCC Components

(\* Plastic material properties)

Material	Density (kg/mm <sup>3</sup> )	Elastic Modulus (GPa)	Poisson's Ratio	Yield Strength (GPa)	UTS (GPa)	% elongation at yield
CR300 LA	7.80E-06	210	0.3	0.3	0.42	26
CR340 LA	7.80E-06	210	0.3	0.34	0.45	23
HR340LA	7.80E-06	210	0.3	0.34	0.45	22
Tested Bumper steel	7.80E-06	210	0.3	*	*	*
Tested Crush Can (CC) steel	7.80E-06	210	0.3	*	*	*

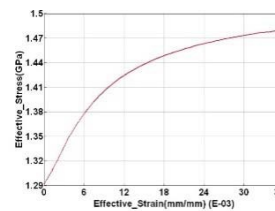


Figure 2. True Stress-Strain for Steel Bumper

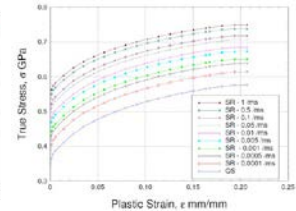


Figure 3. Rate Dependent True Stress-Strain Curve for Crush-Cans

requirements for mass applications of composites in the U.S. automotive industry.

Table 2. High Speed and Low Speed Test Conditions for Steel FBCC

No.	Load Case	Mass (kg)	Speed (mph)
1	Rigid Full (NCAP)	300	35
2	Rigid Offset	321.34	26.54
3	Rigid Angular (30 Degree)	321.34	20.29
4	Rigid Center Pole	306	14.35
5	Pendulum Impact Center	302.3	10.05
6	Pendulum Impact Quarter	326.4	9.5

Table 3. Design Targets for Composite FBCC Design

No.	Load Case	Energy Absorption, EA (kJ)	Average Crush Force (kN)	Crush Distance (mm)
1	Rigid Full (NCAP)	37	220	200
2	Rigid Offset	22	120	200
3	Rigid Angular (30 Degree)	13	90	150
4	Rigid Center Pole	6	N/A	N/A
5	Pendulum Impact Center	3	N/A	N/A
6	Pendulum Impact Quarter	3	N/A	N/A

### 3. Design of Composite FBCC

Over twenty conceptual designs were discussed for the composite front bumper and crush-can system along with material systems and manufacturing processes during the initial phase of the project. A final design for composite FBCC was selected as shown in Figure 4. The design consists of a C-Channel bumper beam section with chopped carbon fiber SMC ribs (to retain rigidity) and a two-piece crush-can with embedded SMC base. To ease NDE (Non-Destructive Evaluation) inspection, crush-cans with flat facets (instead of round or conical shape) were chosen.

The materials and processing systems (MPS) team selected “compression molding” as a primary method to mold composite FBCC components, after initially examining thermoforming and pultrusion for uniform crush-can cross-sections. The key consideration was that compression molded parts can be produced at a high rate which is one of the key

Several details were considered in the design of the FBCC. One key design iteration for the bumper involved the design of the front bumper flanges, as shown in Figures 5-6. It is expected that a bumper will tend to first bend backward and then flex back after any frontal impact. A simulation study, conducted by ESI, concluded that the bumper with flanges performed better than without flanges under certain load conditions. The reverse curl in the bumper flanges (shown in Figure 5) brings the neutral axis to approximately the center of the cross-section and creates equal strains on the front and rear where strain levels are at their maximum.

Another key design iteration for the bumper was the inclusion of a compression molded back-plate, shown in Figure 6. Simulations carried out on FBCC models with back plate proved beneficial for concentrated loads such as pole impacts. Without a back-plate, the force induced by the pole is concentrated locally and cause the bumper material to fail (Figure 7) before the load is transferred to the crush-cans. To avoid such failure, a back plate was modeled and bonded to the flanges of the bumper using. The predictions show that a bumper with back-plate helps distribute the concentrated load throughout the Beam (Figure 8). However, the additional piece and assembly cost of the back-plate, combined with the additional weight led the team to decide to not include this piece in the final FBCC proposal, as it did not add significant value to the objective of correlating the material models, although it did improve performance.

SMC ribs (Chopped Carbon Fiber) co-molded inside the C-channel bumper were designed to

increase flexural rigidity of the bumper and avoid opening of the bumper during crash loads. The SMC ribs were also used to position and constrain the two crush-cans in an adhesive joint with the bumper (as shown in Figure 1).

Different crush-can shapes and reinforcement concepts were considered but a two-piece, conical dodecagonal face crush-can design was eventually selected, which best balanced performance, NDE and manufacturing objectives (Figure 9-10). Flanges on either side of each crush-can were designed to provide bond interface surfaces. Stand-offs were molded into the flanges to maintain a consistent bond-line of 1.0 mm thickness, shown in Figures 11 and 12. Stand-offs were shaped such that the lower flange with 31° depressions will allow upper flange with 30° cone to register on the round end. Holes on crush-can side flanges (Figures 9 and 10) represent rivet locations used to bond crush-can halves in addition to adhesive applied on flat surfaces; whereas, holes on rear flange of the crush-can represent bolt locations used to join the complete FBCC assembly to the back rail of the sled. Crush-can halves are molded to form circular flanges on the front end which will be used as bonding surfaces with the bumper beam (Figure 13). A second plane of bonding is provided via the SMC rib shown in Figure 14. Stand-offs were designed on the external surfaces of SMC ribs to facilitate ease of bonding.

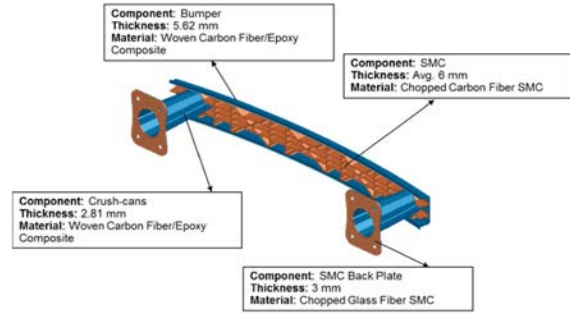


Figure 4. Composite FBCC Design and Material Strategy

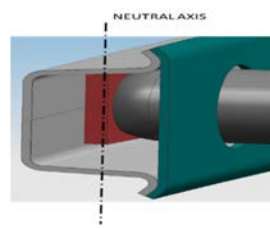


Figure 5. Bumper with Flanges

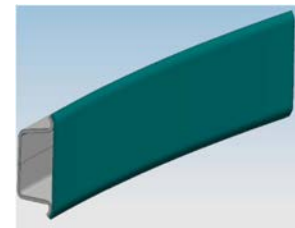


Figure 6. Bumper with Back-Plate

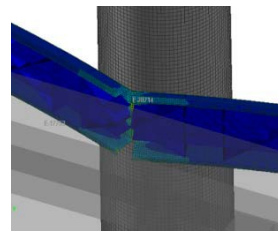


Figure 7. Bumper without Back-Plate

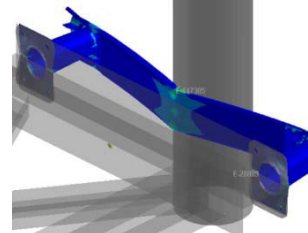


Figure 8. Bumper with Back-Plate

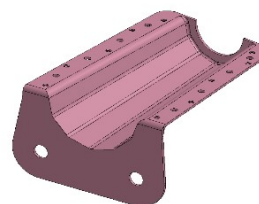


Figure 9. Can Upper Half



Figure 10. Can Lower Half



Figure 11. Stand-Off on Upper Half



Figure 12. Standoff Receiver on Lower Half

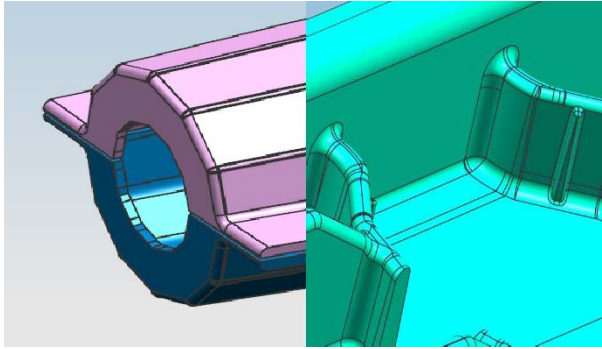


Figure 13. Front End Flange

Figure 14. Standoffs on SMC

As shown in Figures 15 and 16, both crush-cans and bumper were designed to have at least 25 mm run-off extension to avoid resin rich areas while matching the actual CAD.

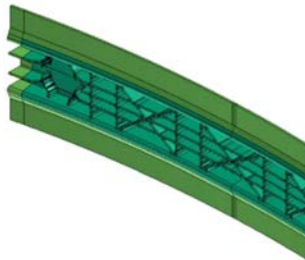


Figure 15. Bumper with Extension

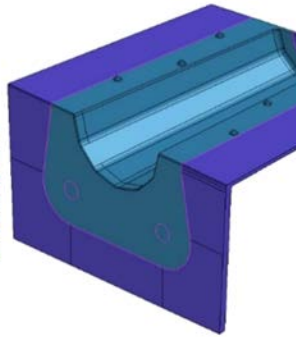


Figure 16. Crush-Can with Extension

#### 4. Finite Element Model

VPS was used to predict the crash performance of the composite FBCC under 6 different load cases as outlined in Table 2.

##### Set up of the model

The finite element model (FEM) for composite parts was developed using 3/4 node shell elements. One multilayered shell was used where each composite layer is accounted for by an integration point through thickness. Figure 17 shows the FEM. The sled was modeled as a rigid body with a point mass of 300 kg at the center of gravity. A target element size of 3.0 mm was imposed to all composite components. A friction coefficient value of 0.3 was used between the wall and the FBCC assembly. The contact force generated between impactor and the composite parts was monitored. The total simulation time for the 70 milliseconds NCAP crash event took about 15 hours to solve using VPS 2015.0 on a 12 CPU workstation.

The SMC ribs inside the bumper are constructed with 3 and 4 node shell elements. The SMC at the rear crush-can was modeled using 8 node brick elements. The crush-cans designs consist of 12 layers of woven carbon fiber with epoxy and the layup for the bumper is a 24-layer woven carbon fiber with epoxy. Table 4 shows individual components with laminate information. The number of plies and sequence chose was based on layer design optimization studies in order to meet performance criteria under axial loads, by simulation, using standard models (here Ladeveze model) available in VPS commercial code. Delamination between two adjacent layers was not modeled, as a single shell with multi-layers was used to represent laminate. In case delamination would occur, the single shell approach would have to be revisited.



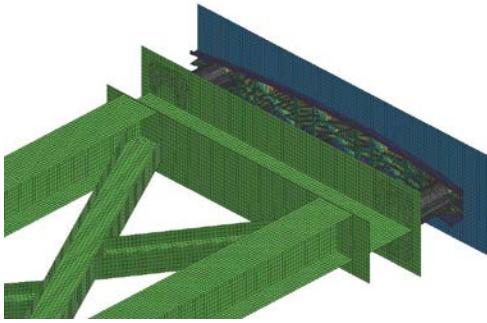


Figure 17. FE Model Illustration for NCAP

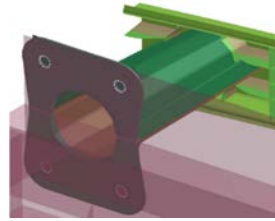


Figure 18. Bolts Connecting Crush-Can to Sled

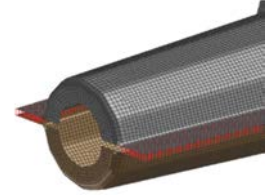


Figure 19. Crush-Can Side Flange Bonding

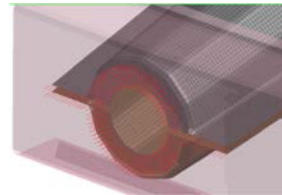


Figure 20. Front CAN-Bumper Tied Link

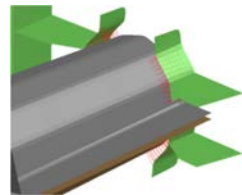


Figure 21. CAN-SMC Tied Link

Table 4. Composite Layup/Thickness

No.	Component	Layup	Thickness (mm)
1	Bumper	[0/45/-45/90/90/-45/45/0] <sub>2s</sub>	5.62
2	Crush-Can	[0/45/-45/90/45/0] <sub>s</sub>	2.8
3	SMC at Bumper	N/A	6
4	SMC at Crush-Can	N/A	3

### Adhesive and assembly modeling

Adhesive bounding has been chosen for composite FBCC. It was assumed according to data from glue producer that no failure would occur in the adhesive bounding and therefore no failure was included in the FE models. The crush-can front section is tied to the bumper and SMC ribs (Figure 20-21). Chopped carbon fiber SMC ribs are integrally molded into the bumper (Figure 22). In FE models, the ribs-to-bumper connection was modeled as coincident node-to-node connection with no failure considered at the interface. Glass fiber SMC used at the rear of the crush-can was modeled as solid elements and the interface between carbon fiber crush-can and glass fiber SMC was represented by 1D bar elements with no interface failure.

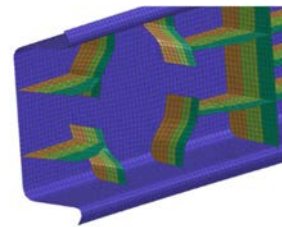


Figure 22. SMC-Bumper Node-to-Node Connection

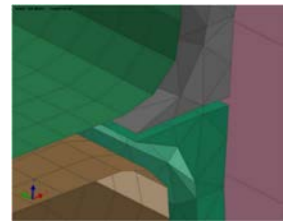


Figure 23. SMC-Crush Can Tied Link

### Material Models and Properties

A continuous damage mechanics model based on Ladeveze model, MAT 131 (\*Multi-Layered Orthotropic Bi-Phase) in VPS has been used to model the progressive damage behavior of carbon fiber/epoxy woven composites. The material properties and parameters of MAT 131 are presented in Table 6.

MAT 131 is a multi-layered composite shell element material model with ply types 1 and 7 used for global ply damage law resp. for Unidirectional (UD) and fabrics. As of today, ply



type 7 only allows perpendicular fibers. Ply type-1 can also be used to approximate woven fabric by stacking two UD layers with appropriate fiber angles and distribution of mechanical properties (Table 7). For the project, Ply Type-1 was used to represent Woven fabric composites.

Ply model TYPE-1 is based on research by P. Ladevèze and E. Ledantec (Ref. [1]) and is modified to include transverse shear by A. Hurez. It corresponds to a homogenized, global description of the fiber and matrix phases. The fiber phase uses a strain-energy based failure criteria for tension and compression. Non-linear (elastic) behavior is possible in compression and is often necessary to account for micro-buckling effects in compression. The shear behavior uses a coupled damage and plasticity model that accounts for modulus reduction and permanent plastic deformations.

Further details on the MAT 131 model can be found in the MAT 131 of VPS User Manual [3]. MAT 105 (\* Elastic-Plastic ITR with ISO Damage) was used to define SMC chopped carbon fibers for ribs in the bumper with properties shown in Table 8. MAT 01 (\*Elastic-Plastic Solid) was used to define SMC chopped fibers located at the rear of Crush-Can with properties as illustrated in Table 9.

Table 5. Elastic Properties of Steel

*MAT	$\rho$ , kg/m <sup>3</sup>	E, GPa	$\nu$
100 (*Null Material Shell)	7.85E-06	210	0.3

Table 6. Material Properties and Parameters of MAT 131

ITYP	RHO	E0t1	E0t2	NU12	Elasticity
1	1.48E-06	1	101.6	0.055	
G012	G023	G012	E0c1	GAMMA	Damage
9.3	4.74	4.74	102.6	0	
EPSifti	EPSiftu	Dftu	IFUND1	ISHD	Plasticity
0.0108	0.0308	0.9	2	2	
EPSifci	EPSifcu	Dfcu			Strain Rate
0.0129	0.0329	0.9			
R0	BETA	m			Failure Model
0.028	1.21	0.4446			
ERATER11	D11	n11	D11r	n11r	
-	-	-	-	-	
FAILDAM	FAILTYP	EPSIslim			
1	0	0.15			

Table 7. Ply Types 1 & 7 in MAT 131<sup>[5]</sup>



Option / Ply type	Representation	Comments
1 (Ply type 1)		Standard representation for UD composite plies
3 (Ply type 7)		Standard representation for woven composite plies: <ul style="list-style-type: none"> <li>Ideally for orthogonal reinforcement</li> <li>Intra-ply shear strains should not be large</li> </ul>

Table 8. SMC Properties for Chopped Carbon Fiber Composites (Shell)

*MAT	$\rho$ , kg/m <sup>3</sup>	G, GPa	$\nu$
105 (*Elastic-Plastic-ITR- with ISO Damage)	1.39E-06	10.47	0.45
SIGM-OPTN	SIGMAy	K, GPa	
Yield Stress	0.16	101.26	
EPSIpmax			
0.015			

Table 9. SMC Properties for Chopped Carbon Fiber Composites (Solids)

*MAT	$\rho$ , kg/m <sup>3</sup>	G, GPa	K, GPa
01 (*Elastic-Plastic-Solid)	1.39E-06	10.47	101.26
SIGM-OPTN	SIGMAy		
Yield Stress	0.16		

## 5. Calibration and component test for the standard Ladeveze model

A single-element and coupon-level simulations were carried out in VPS to calibrate MAT 131 described above. Coupon tests were performed by Delsen Test Laboratories (now known as Delsen division of Element) on two different material systems, UD and Woven Carbon Fiber/Epoxy systems. Additionally, component level (Hat-Plate) calibrations were also carried out in VPS to further validate MAT 131. Hat-Plate axial crush tests were conducted by team members at the University of Michigan.

Single Element and Coupon Calibration of MAT 131 for Ladeveze model

The necessary material properties for stiffness and failure were extracted from standardized tests. The model and input data were then validated using a single element and coupon test case as shown in Figure 24.

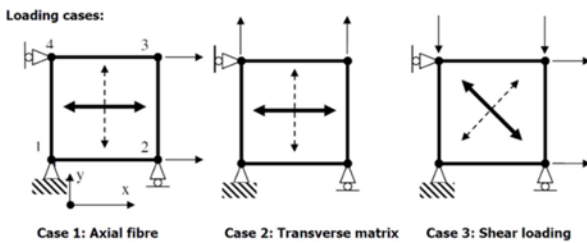


Figure 24. A Single Element Description of FE Model

**Tension Test**

The element was loaded at a constant velocity of 1.0 mm/ms. Five coupons were loaded in the 0° tension direction (=90° direction for a balanced woven fabric composite). Good correlation was found for stiffness and failure data as summarized in Table 10 and Figure 25.

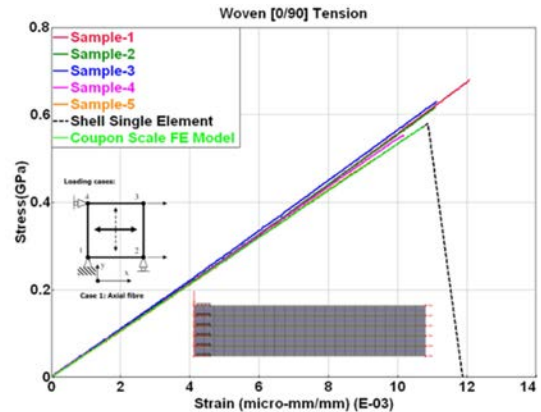


Figure 25. Fiber Tension in [0]° Direction

Table 10. Property Extraction from Test Data for 0° Tension Fiber Direction

Property	Value
$E_1^{0t}$ Tensile Elastic Modulus (Fiber Direction)	50.8 GPa (101.6 GPa for Ply-1)
$\sigma_1^R$ Tensile Failure Stress (Fiber Direction)	580 MPa
$\nu_{12}$ Poisson's Ratio	0.055
$\epsilon_1^R$ Tensile Failure Strain (Fiber Direction)-Initiation	0.0108
$\epsilon_1^R$ Tensile Failure Strain (Fiber Direction)-Ultimate	0.0109
$d_u^R$ Assumed Ultimate Damage (Fiber Direction)	0.9

**Compression Test**

Coupons were also loaded in the 0° direction compression (=90° direction for a balanced woven fabric composite). Some scatter was observed in the test data (Figure 26) but reasonable averages for stiffness and failure data were found as summarized in Table 11.

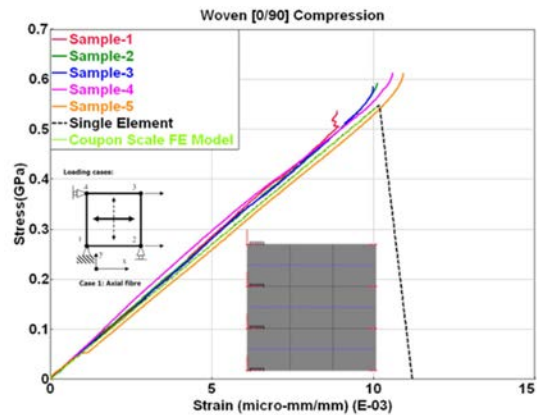


Figure 26. Fiber Compression in [0]° Direction

Table 11. Property Extraction from Test

### Data for 0° Compression Fiber Direction

Property	Value
$E_{1c}^{0c}$ Compression Elastic Modulus (Fiber Direction)	51.3 GPa (102.6 GPa for Ply-1)
$\sigma_{1c}^{0c}$ Compression Failure Stress (Fiber Direction)	619 MPa
$\epsilon_{1c}^{0c}$ Compression Failure Strain (Fiber Direction)-Initiation	0.0129
$E_{u1c}^{0c}$ Compression Failure Strain (Fiber Direction)-Ultimate	0.0130
$d_{u1c}^{0c}$ Assumed Ultimate Damage (Fiber Direction)	0.9

### Shear Test

To capture the shear behavior for woven composites, +/- 45° coupons were cyclically loaded with cycles of 10% ultimate tensile strain (17%, 25%, 37.5%, 50%, 70% and 90%) to get at least five damage points. The average ultimate tensile strain of 1.08% was obtained from 0° degree tension test. The cyclic test was used to extract damage evolution, plasticity and final shear strain data.  $G_{12}^0$  is given by the initial slope of the shear stress ( $\sigma_{12}$ ) versus the engineering shear strain ( $2\epsilon_{12}$ ) curve.

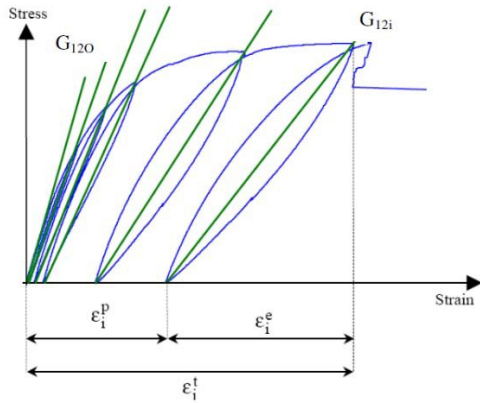


Figure 27. Shear Response via Cyclic Curve (Schematic)<sup>[5]</sup>

Shear damage is given by the change in slope of the cyclic modulus  $G_{12}^i$  with each loading cycle (i). Initial slope of the un-damaged cyclic stress-strain curve gives the initial shear modulus. At each cycle, stiffness loss is characterized by modulus reduction. The degree of shear damage  $d_{12}$  is given by the relationship in Equation-1.

$$d_{12}^i = 1 - \frac{G_{12}^i}{G_{12}^0} \quad (1)$$

The model uses the term  $Y_{12}$  to define damage progression given by relation (Equation-2).

$$Y_{12} = \frac{1}{2} G_{12} (2\epsilon_{12}) \quad (2)$$

From the cyclic curve and above expressions, it is possible to plot the evolution of  $Y_{12}$  vs damage  $d_{12}$  for each loading cycle (i), as shown in Table 12.

Table 12. Shear Elastic Damage Evolution

Cycle	$G_{12}$ (GPa)	$(2\epsilon_{12}^e)$	$d_{12}$	$Y_{12}$
0	9.37	0.00306	0	0
1	8.06	0.00488	0	0.006
2	7.21	0.00771	0.235	0.015
3	6.62	0.01027	0.357	0.022
4	5.64	0.01381	0.423	0.028
5	4.57	0.01620	0.457	0.032
6	4.28	0.01884	0.492	0.038

Plasticity is given by the growth of plastic strains ( $\epsilon_{12}^p$ ). The model uses the term ( $p_i$ ) as a measure of effective plastic strain. The term ( $R_i$ ) is used to evaluate influence of damage ( $d_{12}$ ) to yield stress ( $R_0$ ) in each loading cycle.

$$p_i = \frac{E_{12}^{p_i}}{E_{12}^{p_i-1}} 2(1-d_i)E_{12}^D \quad (3)$$

$$j = \sum_{i=1}^{i=j} p_i \quad (4)$$

$$R_i = \frac{\sum_{j=1}^i p_j}{1 - d_i} - R_o \quad (5)$$

Finally, a curve fitting exercise was performed to fit exponential plasticity function (with parameters  $\beta$  and  $m$ ) to the  $R_i$  versus  $p_i$  curve, Equation-6.

$$R_i = P(p_i)^m \quad (6)$$

Table 13 summarizes plasticity results obtained from the integration and summation equations 3 to 6. A good correlation has been found between test and simulation (Figure 28).

Table 13. Shear Plasticity Behavior for Woven Carbon Fiber/Epoxy Composites

Cycle	$(2\epsilon_{12}^p)$	$(1-d_{12})$	$p_i$	$p_j$	$R_i$
0	0	1	0	0	0
1	0.00019	0.8994	0.000185	0.000185	0.012529
2	0.00087	0.7911	0.000525	0.000710	0.026603
3	0.00221	0.7160	0.000903	0.001614	0.044446
4	0.00471	0.5918	0.001504	0.003118	0.054344
5	0.00856	0.4552	0.001782	0.004900	0.061865
6	0.01328	0.4177	0.001960	0.006861	0.062844

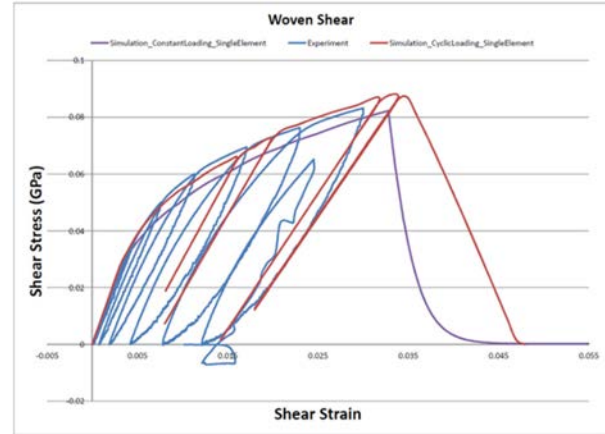


Figure 28. Shear Behavior of Woven Carbon/Epoxy Composites

### Hat-Plate Component Test using standard Ladeveze model

The results obtained using the standard Ladeveze model used in the previous commercial version of VPS are displayed below. They will be complemented and compared vs. the new Waas Pineda progressive damage model developed in the project.

A Hat-Plate design of three different ply configurations (Table 14) was tested in crush loading. The dimensions of the component are shown in Figure 30. The plate was bonded to a hat section on the side flanges using epoxy adhesive from Dow (BETAMATE® 73326/73327). An aluminum block was manufactured with a slot to fit the bottom 25 mm of the part; and a plastic epoxy putty was used to bond the part in the slot (Figure 30).

An Instron Dynatup Impact test machine (Figure 29) was used to crush samples. A mass of 74.5 Kg was dropped from a height of 0.98 meters. Table 14 shows test results for different ply configurations and the corresponding VPS simulation results. The force-deflection overlays of test and VPS simulations are shown in Figures

31-33. Both, in experiments and simulations, it was observed that crush initiates on the front and proceeds rear; however, simulations show large peaks of force during crush followed by instantaneous drop of force. This is a typical behavior in CAE standard models characterized by the sudden deletion of elements until next rows of elements are in contact. This sudden deletion of elements could be attributed to hard contact between the impact plate and the hat-plate composite model, or due to other numerical effect; this behavior will be revisited using the innovative Waas Pineda model shown in next chapters. Figures 31-33 reveals a high frequency noise in the CAE (un-filtered) data than the test data. When plotted against SAE Class 180 filter, it not only smoothens out high frequency signals but also follow closely peaks and valleys of the original CAE signal. An acceptable correlation to test was obtained in terms of the total crush length and the average crush force for QI and Cross-Ply Woven laminates, however, some discrepancy was found for UD/Woven combo laminates.

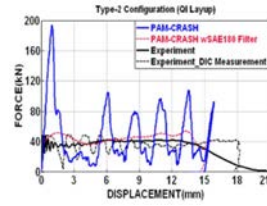


Figure 31. Quasi-Isotropic Woven Laminate

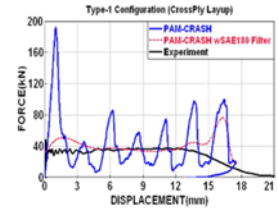


Figure 32. Cross-Ply [0/90] Woven Laminate

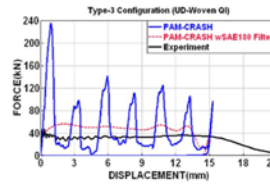


Figure 33. UD/Woven Laminate

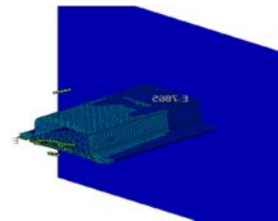


Figure 34. VPS Simulation

Table 14. Axial Crush Test vs Predictions

	QI Woven				0/90 Woven				UD/Woven QI				
Layup for Hat Section	[0/90/45/-45/0/90/0/-45/45/90/0] - 11 Layers				[0/90/0/90/0/90/0/90/0/90/0] - 11 Layers				[0/0/0/90/45/0/0/-45/90/0/0/0] - 11 Layers				
Layup for Plate	[0/90/45/-45/0/90/0/-45/45/90/0] - 11 Layers				[0/90/0/90] - 8 Layers				[0/90/45/-45/0/90/0/-45/45/90/0] - 11 Layers				
SpecimenID	S-1	S-2	Test Avg.	VPS	S-3	S-4	S-5	Avg.	VPS	S-6	S-7	Avg.	VPS
Crush Distance, mm (Test)	18.2	15.5	16.85	15.8	14.5	16.2	17.7	16.13	17.5	20.1	16.3	18.2	15.3
Plateau Load, kN (Test)	41	41	41	44	36	-	36	36	35	35	35	35	50

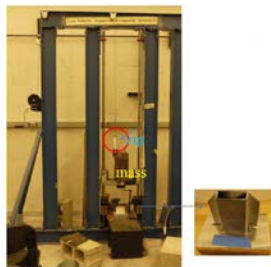


Figure 29. Test Equipment

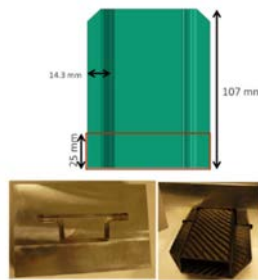


Figure 30. Hat-Plate

## 6. Composite Full FBCC Crash Simulations using standard Ladeveze model

The contact force versus displacement response between wall/impactor and the composite FBCC for each load case are presented in Figure 35-40. Overlays of VPS predictions for the steel FBCC and composite FBCC for the same boundary and initial conditions are also presented.

Experimental tests were not yet available when releasing the paper.

For composites, the initial velocity for the Center-Pole impact load case has been reduced by half in order to withstand complete energy absorption. Unlike steel which undergoes energy absorption via plastic deformation due to its ductile nature, composites absorb a significant amount of energy through cracking



and breaking by due to their brittleness. This phenomenon, was especially evident for the center-pole impact at 14 mph. For composites, there is no “folding deformation” which generally occurs in steel; once a ply fails, elements need to be eroded in order to maintain numerical stability, and the next rows of elements engage in contact; this is evident from the force-deflection curves where element deletion results in a sudden force drop.

The trend in steel and composites behavior is similar where the force increases to peak from the initial impact up to flexing of the Bumper, followed by stable crushing/folding of crush-cans. A complete energy absorption (EA) for both steel and composites was achieved for the same given kinetic energy. The equivalent energy absorption for composites was achieved at a mass savings of nearly 40% as shown in Table 16. Table 15 shows steel and composites FBCC predictions under various load scenarios.

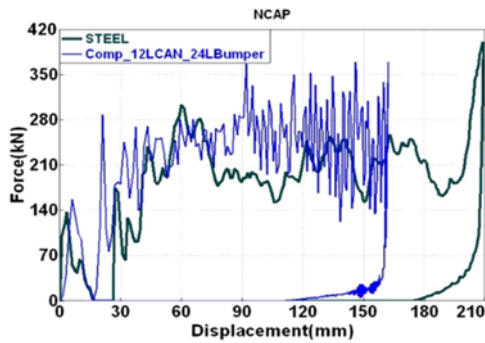


Figure 35. NCAP crash test, composites vs steel

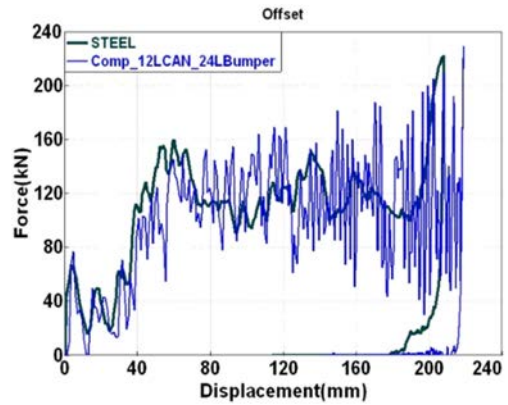


Figure 36. Offset crash test, composites vs steel

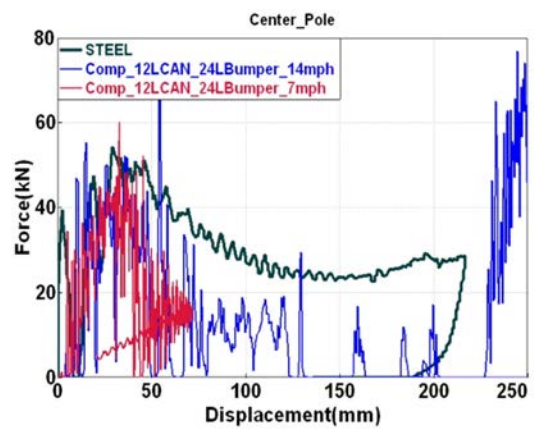


Figure 37. Center Pole crash test, composites vs steel

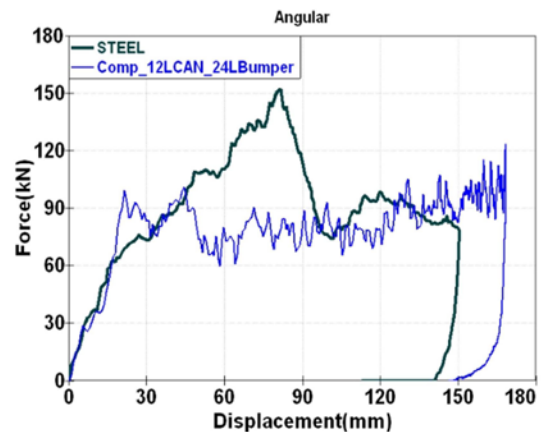


Figure 38. Angular crash test, composites vs steel

Table 15. Steel FBCC vs Composite FBCC Predictions

No.	Load Case	STEEL FBCC Simulations			Composite FBCC Simulations		
		Energy Absorption, EA (kJ)	Average Crush Force (kN)	Crush Distance (mm)	Energy Absorption, EA (kJ)	Average Crush Force (kN)	Crush Distance (mm)
1	NCAP	36	220	200	35	250	162
2	Offset	22	120	200	22	120	218
3	Angular	13	90	150	13.2	88	165
4	Center Pole	5	N/A	N/A	3	N/A	N/A
5	Pendulum Impact Center	3	N/A	N/A	2	N/A	N/A
6	Pendulum Impact Quarter	3	N/A	N/A	2	N/A	N/A

Table 16. Mass Comparison between Steel FBCC and Composite FBCC

Component	Total Mass (Kg)
<b>STEEL</b>	
Steel Bumper	5.27
Steel Crush-Cans	1.84
Front Bracket	0.93
4 Additional Bumper Attachments	0.26
Rear Bracket	2.7
2 Additional Rear Bracket Attachments	0.29
<b>Total Mass</b>	<b>11.29</b>
<b>Total Mass Without Additional Attachments</b>	<b>10.74</b>
<b>COMPOSITE</b>	
Bumper 24 Layers	2.76
Crush-Cans 12 Layers	1.0
SMC Ribs in Bumper (7-5 mm Thick)	1.88
SMC Rear (~ 3 mm Thick)	0.21
<b>Total Mass</b>	<b>5.85</b>
Mass Savings Over Steel	<b>48.18%</b>
Mass Savings Without Additional Attachments	<b>45.53%</b>

Manufacturing defects could have a significant influence on the crash performance of structural composite parts. PAM-FORM and Fibersim can be used to consider ply mechanical data, process conditions and other factors which can be input into the CAE model to improve the discrete characterization of individual elements in the model to consider processing effects and better account for induced instabilities in the design from the manufacturing process [Ref. 9].

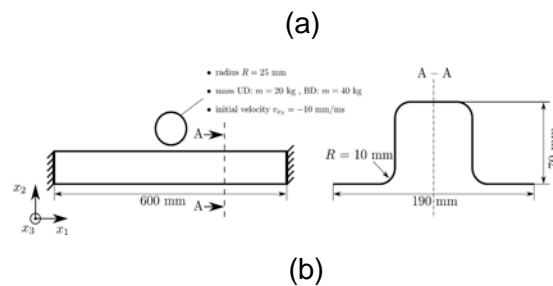
An additional source of uncertainties lies in the modeling of assembly especially bounding rupture which would need further work.

## 7. Implementation and validation of the Waas Pineda composite crash model

### Mesh dependency of composite crash simulation results

A crucial part of virtual composite prototyping of crash structures is the proper prediction of the energy absorption under progressive damage evolution. Phenomenological based continuum damage models are most common used to describe the failure mechanisms of composite materials (Ladeveze et al. Ref. [1]). However, it has been shown that these models exhibit a strong mesh dependency caused by their local continuum based formulation.

To illustrate this deficiency, the lateral impact of an omega shaped UD reinforced composite profile has been analyzed using different mesh densities. The model setup and the impact force-displacement curves are shown in Figure 39. The results have been obtained using a Ladeveze composite model in ESI VPS.





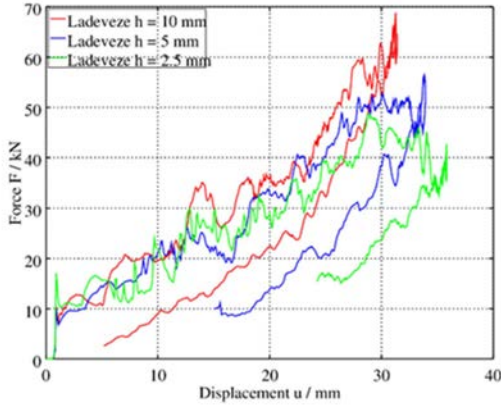


Figure 39. Lateral crash of a omega shaped UD composite profile: (a) model setup and (b) impact force-displacement curves for three distinct mesh sizes.

It can be seen that both the impact force and the impact distance changes depending on the mesh density. To overcome this deficiency a new hybrid composite damage model has been implemented in ESI VPS. It utilizes the well-established elasto-plastic composite description of the Ladeveze model and combines it with a new cohesive damage approach. The fundamental relations of the model are summarized in the following section.

Presentation of the hybrid composite model (Waas Pineda)

The energy absorption of composite crash structures is substantially driven by characteristic damage mechanisms, such as – delamination, matrix cracking and fiber breakage. A robust modelling of these phenomena is there for a crucial part of the virtual prototyping process. Since classical local continuum damage models show a strong mesh dependence, a new hybrid approach has been implemented in the commercial FE package ESI Virtual Performance Solution (VPS). It is based on the works of Pineda & Waas Ref. [8]and utilizes the internal transition from the

continuum based constitutive relations to a cohesive traction-separation law (cf. Figure 40).

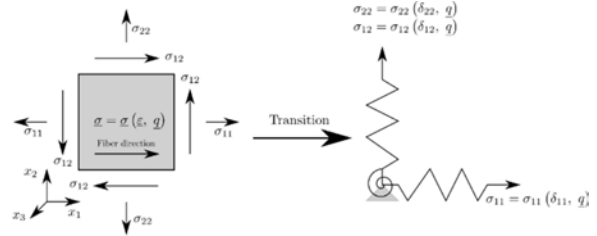


Figure 40. Internal transition from continuum stress-strain relation to a cohesive traction-separation law.

In the continuum state an elasto-plastic material model is utilized to define the stress response

$$E^{el} = \begin{matrix} E_{11} \\ E_{22} \\ E_{12} - E_{12}^{pl} \end{matrix} = S <$$

with  $E^{el}$  the elastic strain vector,  $<$  the corresponding stress vector and  $S$  the anisotropic elastic compliance matrix. The evolution of the plastic shear strain  $E_{12}^{pl}$  is defined by a Hill-type yield function

$$f(a_{12}, R) = |a_{12}| - R(E_{12}^{pl})$$

with the

$$R(E_{12}^{pl}) = R_0 + \beta (E_{12}^{pl})^m$$

the hardening function and  $R_0$  the initial yield stress,  $\beta$  the hardening law multiplier and  $m$  the hardening law exponent.

The transition to the cohesive state is subsequently based on the definition of a characteristic element length ( $l_1^e$  and  $l_2^e$ ) and the elastic strain equivalent separations

$$a_{11} = l_1^e E_{11},$$

$$a_{22} = I_2^e E_{22},$$

$$a_{12} = \frac{1}{2} I_2^e (E_{12} - E_{12}^{pl}).$$

$$a_{22}^f = \frac{2G_{IC}^2}{Y},$$

$$a_{12}^f = \frac{2G_{IIC}}{Z}.$$

A stress based criteria is used to identify the transition point for the 3 damage modes (1<sup>st</sup> and 2<sup>nd</sup> fiber damage and inplane shear damage) individually

$$\left(\frac{\sigma_X}{\sigma_X^f}\right)^2 = 1$$

$$\left(\frac{\sigma_Y}{\sigma_Y^f}\right)^2 = 1$$

$$\left(\frac{\sigma_Z}{\sigma_Z^f}\right)^2 = 1$$

with  $X$ ,  $Y$  and  $Z$  the corresponding material strength. The subsequent cohesive stresses are given by

$$a_{ij} = \begin{cases} K_{ij} a_{ij} & a_{ij} < a_{ij}^0 \\ (1 - D_j) K_{ij} a_{ij} & a_{ij}^0 < a_{ij} < a_{ij}^f \\ I & a_{ij}^{res}, \quad a_{ij} > a_{ij}^f \end{cases}$$

with  $a_{ij}^0$  and  $a_{ij}^f$  the separations at damage onset and total failure, respectively and  $K_{ij}$  the cohesive stiffness. While the damage onset separation results naturally from the deformation state at damage initiation, the separation at total failure is governed by the fracture toughness of the damage modes ( $G_{IC}^1$ ,  $G_{IC}^2$  and  $G_{IIC}$  respectively)

$$a_{11}^f = \frac{2G_{IC}^1}{X}$$

## MATERIAL CALIBRATION

While standard experiments can be used to parametrize the continuum material model, additional tests are required to examine the fracture toughness of the material.

### **In-plane elasto-plastic calibration**

The necessary material properties for stiffness and failure were extracted from standardized tests. The model and input data were then validated using a single element and coupon test case as shown in Figure 41.

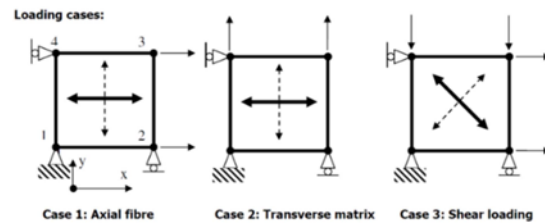


Figure 41. A Single Element Description of FE Model

**Tension Test** The element was loaded at a constant velocity of 1.0 mm/ms. Five coupons were loaded in the 00 tension direction (=900 direction for a balanced woven fabric composite). Good correlation was found for stiffness and failure data as summarized in Table 10 and Figure 42.

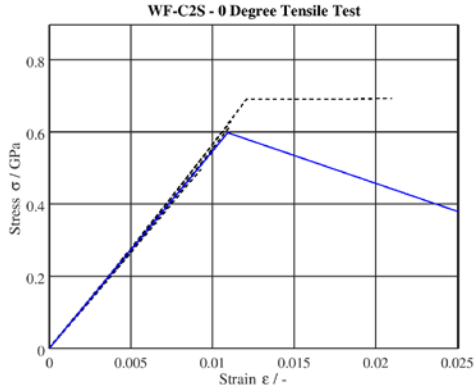


Figure 42. Fiber Tension test in  $[0]^\circ$  Direction (black dashed curves) in comparison with the VPS model response (blue curve)

Property	Value
$E_{11}^T$ $0^\circ$ tensile modulus	54.67 GPa
$X^T$ $0^\circ$ tensile strength	597.7 MPa
$\nu_{12}$ In-plane Poisson's ratio	0.055

Compression Test Coupons were also loaded in the  $0^\circ$  direction compression ( $=90^\circ$  direction for a balanced woven fabric composite). Some scatter was observed in the test data (Figure 43) but reasonable averages for stiffness and failure data were found as summarized in Table 18.

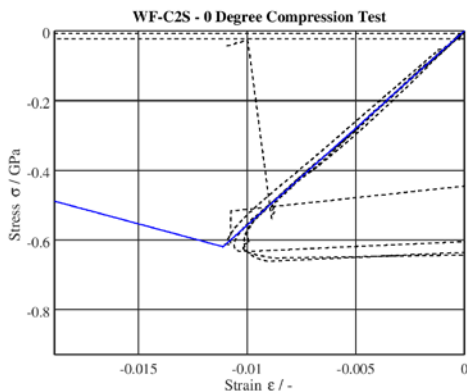


Figure 43 : Fiber Compression test in  $[0]^\circ$  Direction (black dashed curves) in comparison with the VPS model response (blue curve)

Property	Value
$E_{11}^C$ $0^\circ$ compression modulus	54.67 GPa
$X^C$ $0^\circ$ compression strength	618.9 MPa

### Inplane Shear Test

To capture the shear behavior for woven composites, V-notched shear tests have been performed. The results are shown in figure 44. The initial slope has been used to identify the initial shear modulus  $G^0$ . The extracted parameters are summarized in Table 19.

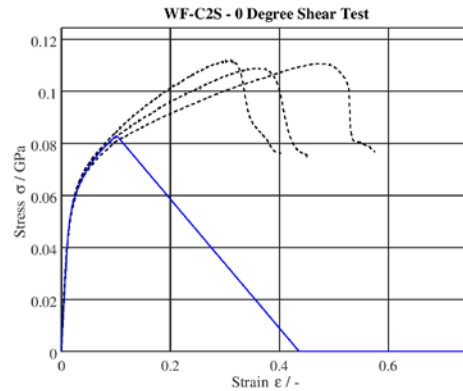


Figure 44. V-notched shear test : experimental stress strain curve in comparison with the VPS model response (blue curve).

Property	Value
$G_{12}^0$ In-plane Shear modulus	3.845 GPa
$R_0$ Initial yield stress	34.78 MPa
$P$ hardening law multiplier	0.10675
$m$ hardening law exponent	0.314268
$Z$ In-plane shear strength	82.9 MPa

**Fracture toughness test** The fracture toughness of the material has been examined using single edge notched tension specimens (cf. Figure 45). The tests have been performed by the McCormick School of Engineering at Northwestern University. The crack propagation has been monitored using digital image correlation. The strain energy has been derived using the  $J$ -integral computation. Combining both data allowed for the identification of the mode I fracture toughness as

$$G_{Ic} = 74 \text{ N/mm}$$

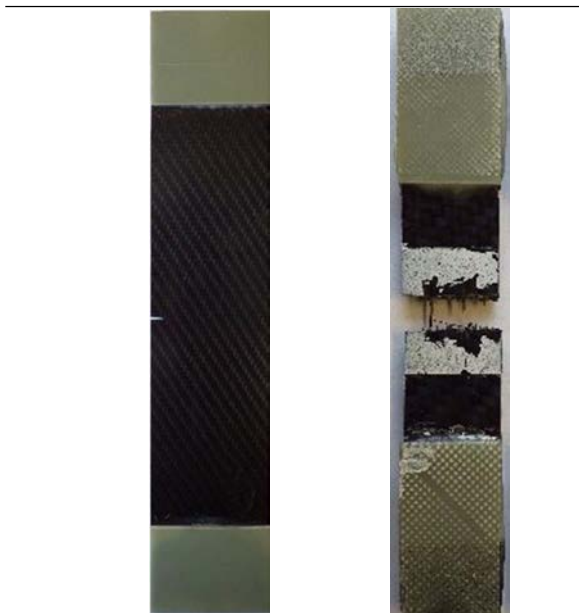


Figure 45. Unfractured and fractured Single Edge Notched Tension Specimen for fracture toughness testing as tested by McCormick School of Engineering at Northwestern University.

#### Coupon test validation

In order to examine the mesh size sensitivity of the new hybrid composite material model, a series of tensile coupon tests with different mesh sizes have been performed. The individual models are shown in Figure 46. The resulting

force-displacement of a classical strain based continuum damage model. It can be seen that no convergence upon mesh refinement is achieved for the continuum approach due to a strain localization. The hybrid cohesive damage model in contrast releases the same amount of energy for all tested mesh sizes.

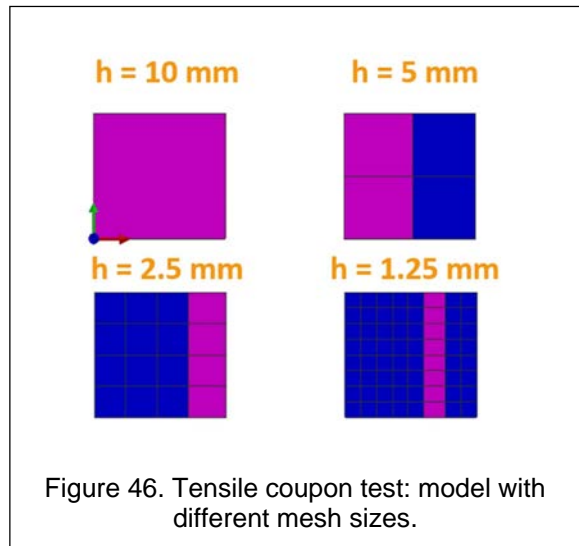
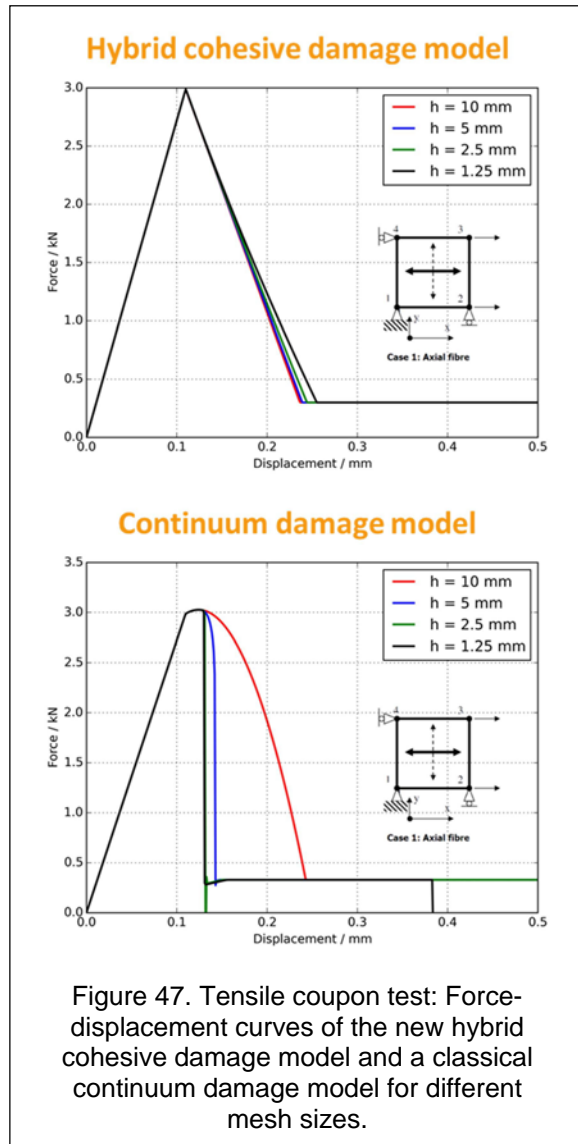


Figure 46. Tensile coupon test: model with different mesh sizes.



### Composite crash test on a omega shaped component

The previously introduced lateral crash model of an omega shaped composite profile has been once again simulated with the new hybrid approach. Using the same three mesh densities as before results in the impact force-displacement curves shown in Figure 48. It is clear that the mesh dependency has been greatly reduced.

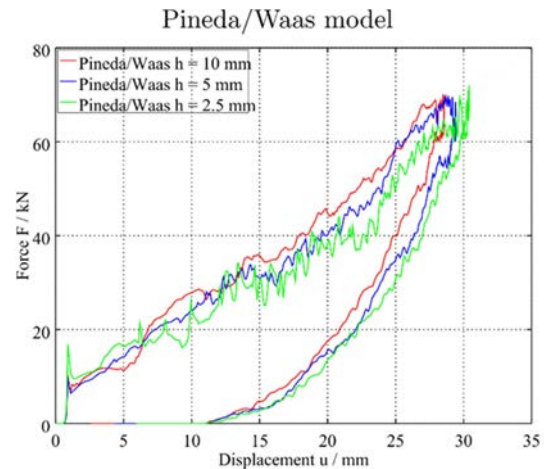


Figure 48. Lateral crash of a omega shaped UD composite profile: impact force-displacement curves for three distinct mesh sizes

### Hat-Plate crash calibration

A Hat-Plate design of three different ply configurations was tested in crush loading. The dimensions of the component are shown in Figure 30. The plate was bonded to a hat section on the side flanges using epoxy adhesive from Dow (BETAMATE® 73326/73327). An aluminum block was manufactured with a slot to fit the bottom 25 mm of the part; and a plastic epoxy putty was used to bond the part in the slot (Figure 49).

In the present contribution only the bidirectional layup of 0/90 Woven layers will be analyzed. The hat and the plate were made from 11 and 8 symmetrically arranged woven layers, respectively.

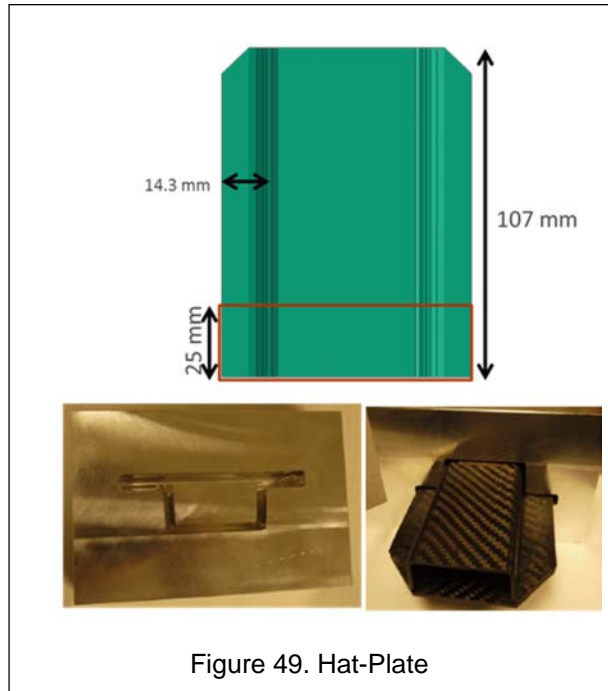


Figure 49. Hat-Plate

A numerical model of the crash structure has been setup in ESI VPS using the previously identified material parameters. Two distinct mesh sizes of 2.5mm and 1.25mm have been analyzed in order to examine the consistency of the simulation results upon mesh refinement. The obtained impact force-displacement curves are shown in Figure 50 in comparison with the experimental results. The deformed crash can models after impact can be seen in Figure 51.

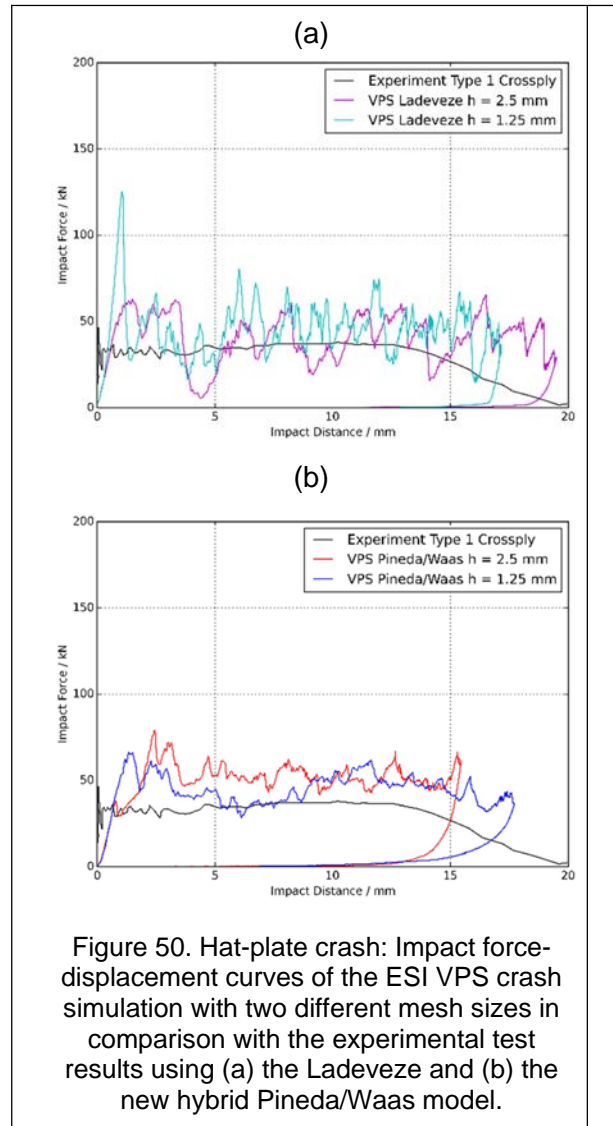


Figure 50. Hat-plate crash: Impact force-displacement curves of the ESI VPS crash simulation with two different mesh sizes in comparison with the experimental test results using (a) the Ladeveze and (b) the new hybrid Pineda/Waas model.

An overall good agreement has been found between for the response of the two mesh sizes in terms of the impact force level. The deflection in the impact distance is mainly caused by the number of eliminated elements during the simulation in order to assure numerical stability. An improvement of the elimination criteria in order reduce the impact on the numerical results is under current investigation. A reduction of oscillations in the impact force-displacement curves illustrates the capability of the model to predicting a gradual energy release.



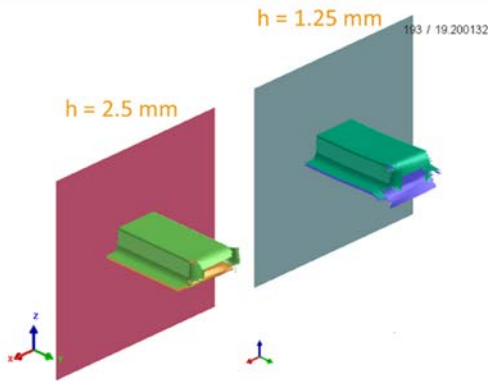


Figure 51. Hat-plate crash: Final deformation of the crash can after impact for the two mesh sizes using the new hybrid Pineda/Waas model.

## Conclusion and recommendations

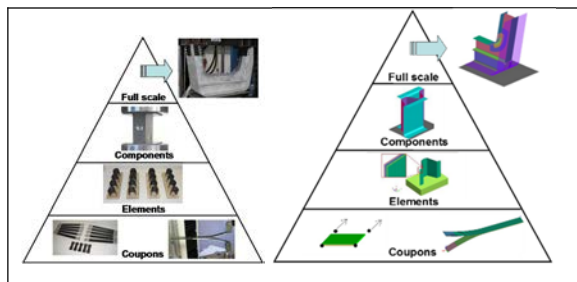


Figure 52. Building block pyramid approach for composite simulation aided design

The purpose of this project was to assess the potential for reducing the weight of a front bumper by replacing steel with composite materials, without any compromise on crash performance.

The front beam was entirely redesigned in order to maximize the benefit of using composite materials. The geometry was redefined accordingly and rib reinforcements as well as assembly strategies were introduced, all based on simulations run with VPS.

The project confirmed that the standard workflow for metals can't be transferred as

such for composites and that in particular material coupon tests are not sufficient to obtain a predictive model for composite crash.

This is due to several factors: composite is not a standard ductile material but consumes crash energy by breaking into pieces. Modelling these phenomena with standard continuum based models reveals the limitation of the continuum approach. A strong mesh size dependence has been found caused by damage localization.

An improved constitutive model introduced by Waas & Pineda, now available in VPS, overcomes this deficiency by the introduction of a cohesive damage approach.

Mesh dependency is largely reduced, nevertheless some work has still to be carried out regarding element elimination strategies.

Also a component test (such as crash can test) is needed as an intermediate step before the full scale prediction because of assembly problematics.

Adhesive bounding models and local rupture effects around connectors, including 3D effects, were not in the scope of this paper. They are nevertheless critical for predictive full scale simulations.

Last but not the least, the manufacturing history of the composite material especially regarding fiber placement and shearing effect in fabrics must be considered.

Despite uncertainties, a good correlation for frontal crash on components like hat section was obtained when following the building block pyramid approach. This enables to reduce the



number of hardware tests required for crash design of composite structures.

## Acknowledgements

This program is supported by the U.S. Department of Energy under Cooperative Agreement Number DE-EE0005661 awarded to the United States Automotive Materials Partnership. Neither the United States Government nor any agency thereof, nor any of their employees, makes any warranty, express or implied, or assumes any legal liability or responsibility for the accuracy, completeness, or usefulness of any information, apparatus, product, or process disclosed, or represents that its use would not infringe privately owned rights. Reference herein to any specific commercial product, process, or service by trade name, trademark, manufacturer, or otherwise does not necessarily constitute or imply its endorsement, recommendation, or favoring by the United States Government or any agency thereof. The views and opinions of authors expressed herein do not necessarily state or reflect those of the United States Government or any agency thereof.

## REFERENCES

[1] Ladevèze P, Le Dantec E, "Damage Modelling of the elementary ply for laminated composites", *Composites. Science and Technology*, Vol. 43, Issue 3, 1992, pp. 257-267.

[2] A.K. Johnson, A.K. Pickett and P. Rozycki, "Computational methods for predicting impact damage in composite structures", *Composites Science and Technology*, Vol-61 (15), pp. 2183-2192, 2001; concluding Reference [2].

[3] VPS (Virtual Performance Solution) Solver Reference Manual, ESI Group, Vol1-6, Version 2016.0.

[4] PAM-QUICKFORM User Guide-Solver, ESI Group, Version 2011.

[5] A.K. Pickett, "Composite Global Ply Model 131 for Elastic, Damage and Failure", ESI GmbH/Institute for Aircraft Design, Stuttgart, September 2012.

[6] A.K. Pickett, "Impact and Crash Simulation of Composite Materials-Training", ESI GmbH, Eschborn, Germany, March 2009.

[7] V.Klesher, R.Zemick, T.Kroupa, "Identification and Verification of the Composite Material Parameters for the Ladeveze Damage Model", University of West Bohemia in Pilsen, Department of Mechanics, Czech Republic, April 2011.

[8] E.J.Pineda, A.M.Waas,"Numerical Implementation of a Multiple-ISV Thermodynamically Based Work Potential Theory for Modeling Progressive Damage and Failure in Fiber-Reinforced Laminates, December 2011.

[9] C.C. Chou, J.Le, P.Chen, D.J. Bauch, "Development of CAE Simulated Crash Pulses for Airbag Sensor Algorithm/Calibration in Frontal Impacts", Ford Motor Company, Research and Vehicle Technology, U.S.A. 301.

[10] X.Jin, "US-3 Validation of Material Models: Composite Fabric Manufacturing Studies by Simulation and Experiment", SPE-Automotive Composite Conference, Novi, MI 2016.

[10] Z. P. Bažant, B. H. Oh, "Crack band theory for fracture of concrete", *Mater Struct*, pp. 155-177, 1983.

